

Experimental Study on Properties of Masonry Infill Walls Connected to Steel Frames with Different Connection Details

Mehdi Kahrizi and Mehrzad TahamouliRoudsari*

Department of Civil Engineering, College of Engineering, Kermanshah Branch, Islamic Azad University, Kermanshah, Iran

*Corresponding Author: Mehrzad TahamouliRoudsari. Email: tahamouli@iauksh.ac.ir

Received: 01 July 2019; Accepted: 27 November 2019

Abstract: The properties of infills and the way they are connected to frames may have significant effects on the seismic behavior of the structure. This study presents an experimental study on evaluation and testing of five single story, single bay samples with the scale 1:3. This study strives to evaluate the behavior of masonry infill walls encased in steel frames, with emphasis on different details of the connection of the wall to the frame. Four frames with masonry infills and one frame without infill are experimented on by applying lateral load to their upper beams. Different details of the connection between the infill and the frame including anchorless wall within the frame, connecting the frame and the infill using separating vertical angles, steel rebars embedded in the infill wall and also using Added Damping And Stiffness (ADAS) elements between the infill and the frame were investigated. The results indicate that the manner in which the infill and the frame are connected not only can significantly affect the crack formation pattern and the failure modes of the infill wall, it's also alters the stiffness, the strength, the ductility, the out-of-plane deformation, and the amount of energy dissipation of the frame. Furthermore, not only using the ADAS yielding damper in the connection between the infill and the frame increases ductility and prevents the load-displacement diagram from plummeting, it also can be used in regions with medium to high relative seismic risk given that it can be replaced after the occurrence of earthquakes.

Keywords: Masonry infill wall; steel frame; wall-frame connection; experimental study

1 Introduction

In most buildings with steel or RC frames, to parcel out the inner space and also to separate the inside space from the outside of the building, masonry walls are used as infills in the frames building. The existence of masonry infill walls can have both beneficial and detrimental effects on the seismic performance of building frames. When the structure is subjected to lateral force, the infill wall tends to connect with the frame surrounding it which can result in different forms of failure in and out of the plane of the frame. Also, the mutual effects of the infill and the frame increase the lateral stiffness of the structure and can considerably change its seismic response.



This work is licensed under a Creative Commons Attribution 4.0 International License, which permits unrestricted use, distribution, and reproduction in any medium, provided the original work is properly cited.

In most of the previous earthquakes, it has been observed that masonry infills either crack or fall down and this, in numerous instances, has caused the loss of life and property. Considering the performance level of the structure, crack formation or local failure is unavoidable. However, the complete destruction of the wall is something that cannot be tolerated. Thereupon, providing methods for anchoring infill walls and preventing them from being destroyed in such a way that the structure can maintain its desirable performance seems necessary.

Since the middle of the 20th century, extensive numerical and experimental studies have been conducted on frames incorporating masonry infill walls subjected to lateral loads and based upon the results, building codes have put forth new criteria. Some of these recommendations can be seen in FEMA 306 and FEMA 356 [1,2] guidelines. Stafford-Smith [3,4], through extensive experimental studies on the strength and the lateral stiffness of masonry infills, recommended the use of the equivalent diagonal strut to model the frame with masonry infill wall.

Complete reports of the studies on frames incorporating infills between 1987 and 2000 have been presented by Moghadam et al. [5], Abrams [6], Calvi et al. [7] and Crisafulli [8]. In these reports, information such as the distribution of stress and strain in the infill, failure modes of infilled frames, the mutual effect of frame and infill, the effect of infills on the stiffness and the strength of the frame and also the effects of the existence of openings were assessed.

A new analytical method to evaluate the shear strength and the cracking pattern of the panel of the infill wall was presented by Moghadam et al. [9]. Eleven frame samples with masonry and concrete infills were tested under cyclic static loads. The results showed that contrary to masonry infills, the failure of the corners is the dominant failure mode in the concrete infills. In order to improve the proposed equations for replacing masonry infills with the equivalent strut, Puglisi et al. [10,11] proposed a plastic concentrators model based on the elasticity theory. Also, the cracking patterns and the failure mechanisms of infill walls were investigated in the modeling of masonry infills. Mohammadi et al. [12] reported the results obtained from an experimental study on a number of frames with high ductility and high strength engineering infills. In these frames, a sliding frictional fuse was added to the infill which increased the ductility and reduced the loss of strength.

Based on energy concepts, Bayat et al. [13] investigated the far-field seismic behavior of structures equipped with ADAS (Added Damping and Stiffness). In that study, three 3-bay samples (5-story, 10-story, and 15-story) with CBF braces with/without ADAS dampers were selected. Three earthquake records were used to carry out the nonlinear time-history analyses and the conclusions were drawn based upon the energy criterion. The results of the study showed that using ADAS dampers results in the dissipation of a large amount of energy imposed on the structure.

In another study and based on energy concepts, Bayat et al. [14] studied the behavior of structures with ADAS dampers, located in the near-field of different earthquakes. In this study, a braced steel frame with yielding dampers was analyzed. The results showed that using ADAS dampers in structures with 5~10 stories causes a significant decrease in the seismic response of the structure to near field earthquakes.

To investigate the behavior and the capacity of rigid masonry infills enclosed in steel frames, Liu et al. [15] tested 14 samples in an experimental study. The results indicated that the presence of axial load significantly increases the lateral strength of the infill. Jazany et al. [16], in an experimental-analytical study, assessed the effects of masonry infills on the behavior of frames with special concentric braces. The results of the study revealed that the presence of the masonry infill wall can increase the lateral stiffness and the load bearing capacity of frames with special concentric braces by 33% and 41%, respectively.

Bayat et al. [17] evaluated the performance of special moment-resisting frames (SMRF) equipped with energy dissipating devices. The energy dissipating elements in the studied structures were ADAS dampers.

The behaviors of these structures and their responses to near-source ground motions were evaluated using nonlinear time-history analyses and the results were presented based on the energy criterion. The effects of change in the PGA and height of the frames on the seismic response of the structures were also evaluated.

The behavior of confined masonry walls under the influence of lateral loads was investigated by Okail et al. [18]. The experimental results showed that the strength of the masonry blocks and the level of confinement play an important role in increasing the ultimate strength and the ductile displacement of the wall. Also, Essa et al. [19] took the effect of the masonry infill wall on the ductility and the behavior of high-strength RC frames under consideration. The studied parameters in the study included comparing the existence and nonexistence of the infill, changing the thickness of the infill, and changing the type of the masonry block.

In another study, the seismic response and the failure mechanism of the infill of a two-story, two-bay RC structure with five different infill configurations were probed. In this investigation, Yuen et al. [20] found that the integrity and the order of the panel of the infill influence the seismic performance of the structure. Jiang et al. [21] examined seven single-story, single-bay RC frames with the following infill configurations: without infill, having infill with rigid connection, having infill with flexible connection. The results showed that in the infill wall with the flexible connection the lateral strength, stiffness, and energy dissipation significantly attenuate but ductility increases.

In order to investigate the out-of-plane response of infill walls, Furtado et al. [22] carried out an experimental test on full-scale infill walls with and without previous planar damage. The important results of the experiment including the hysteretic load-displacement diagram, crack formation phases in the wall, stiffness reduction, and energy dissipation were reported. In another study carried out by Basha et al. [23], the behavior of 11 samples of masonry infills in RC frames subjected to cyclic static lateral loads was experimented. The results showed that in most cases the failure of the column is due to the shear force, even if the infill wall is weak.

In an experimental and numerical study, Kahrizi et al. [24] investigated the parameters influencing the behavior of masonry infill walls connected to steel frames via ADAS yielding dampers. That study, the experimental results of three single-story single-bay frames were presented. Then, numerical models of the samples were verified in ABAQUS in order to assess the different parameters affecting the behavior of the frames with ADAS dampers. The effects of each of these parameters on the stress distribution, failure modes of the wall, stiffness, strength, ductility, and energy dissipation were evaluated.

Because of the wide utilization of masonry infill walls in conventional buildings, studying the effects of the wall on the behavior of the structure during earthquake is a practical and important subject. Because of the brittle nature of the materials of the masonry infill, this structural element undergoes premature failure which inevitably leads to a drastic decline in the lateral load bearing capacity of the structure. Also, studying the previous earthquakes shows that the lack of connection between the infill wall and the frame has brought about the early failure of the wall which has resulted in significant losses of life and property. Although numerous studies on the effects of the infill wall on the behavior of the frame can be found, very few investigations have been conducted on the effects of the connection between the frame and the infill.

To that end, in this study, the behavior of masonry infill walls confined in steel frames under the influence of lateral loads and with different types of infill-frame connection was experimentally examined. Five single-story, single-bay frames with the scale 1:3 were subjected to in-plane monotonic lateral displacement at ceiling elevation. Four of the frames incorporated masonry infill walls and one did not have an infill wall. Different details of the connection between the infill and the frame including the connection between the wall and the unanchored frame, connecting the wall to the frame by using vertical separating angles, bracing the infill wall to the frame using embedded steel rebars and finally placing an ADAS damper between the infill and the frame in one of the samples were investigated.

The main parameter of this study is the manner in which the infill wall and the frame are connected. The results suggest that the type of the connection between the infill and the frame affects the stiffness, the strength, the ductility, the out-of-plane movement, and the cracking pattern of the wall. Adding the ADAS yielding damper and its connection to the infill and the frame causes ductility to increase and also prevented the load-displacement diagram of the frame from plummeting. Therefore, considering the suitable performance and the capacity to be replaced after an earthquake, it is recommended that as a suitable detail.

2 Description of Experiment

2.1 Test Samples

Five single-story, single-bay steel frames the scale 1:3 the span length of 1790 mm and the elevation of 1200 mm were constructed and were subjected to in-plane uniform cyclic static lateral load. The infill wall was built using imperforated bricks the dimensions $210 \times 110 \times 66$ mm and the thickness of the panel was 110 mm in all of the samples. The columns and the beam were respectively built of IBP 120 and IBP 100 profiles and the beam and the column were rigidly connected using joint penetration groove welding.

The frame has two base plates with the dimensions $350 \times 250 \times 20$ mm to attach it to the lower chassis. The columns were to be rigidly connected to the base plates and to achieve this, stiffening plates with the height of 100 mm and the thickness of 10 mm were used to annex the webs and the flanges of the columns to the base plates. A plate with the dimensions $1140 \times 250 \times 8$ mm was put underneath the wall in the space between the base plates which was connected to the two base plates on both sides.

To investigate the effects of the connection between the plate and the infill on the seismic behavior of the frame, five different samples were tested whose material properties and detailed geometry are presented in [Tab. 1](#) and [Fig. 1](#), respectively. One sample without an infill wall, one sample with an infill wall but without any kind of connection between the frame and the panel of the infill, and three samples with different frame-infill panel connections were chosen and tested.

Table 1: Specifications of the experimental samples

Sample number	Name of the sample	Sample description
1	BF	Frame without infill wall
2	SF	Frame with a complete infill and without any kind of connection between the infill and the frame
3	CF-1	Frame with infill wall braced with vertical angles
4	CF-2	Frame with infill wall braced with embedded steel rebars
5	CF-3	Frame with infill wall braced with a secondary frame and ADAS yielding damper

In the CF-1 sample, by a margin of 50 mm, the wall was completely separated from the columns on its two sides using for angles with the dimensions $40 \times 40 \times 4$. Using appropriate welding, the angle attached to the bottom of the beam at the top and to the baseplate at the bottom. These angles, in addition to separating the wall from the columns of the frame, resist against the out of plane movement of the wall.

The frame of the CF-2 sample includes six 8 mm steel rebars with the total length of 600 mm, with a 90° bend on each end, one with a length of 100 mm to be connected to the column and the other with a length of 50 mm to be placed in the vertical mortar joint. These steel rebars firmly welded to the column and placed in the fifth, eighth, and eleventh rows to provide the stability for the wall and keeping it from moving outside of

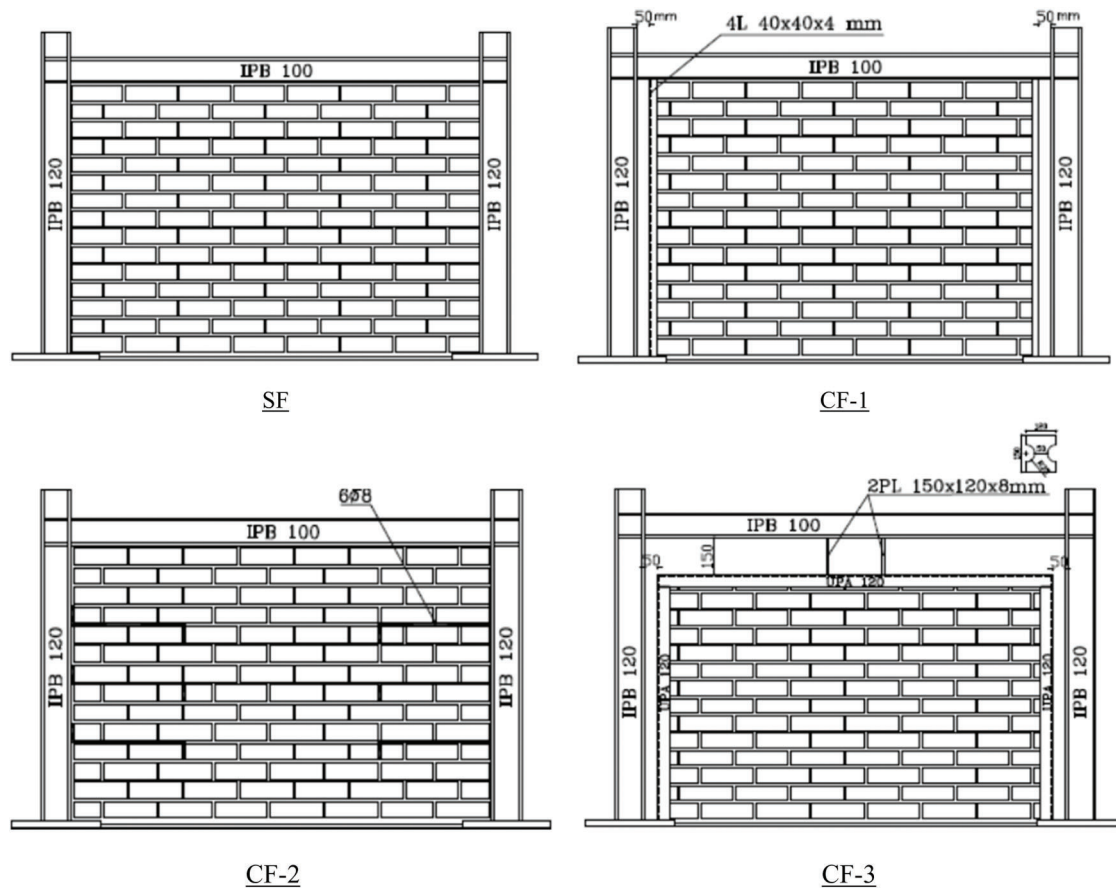


Figure 1: Geometry and the shapes of the experimental samples

its plane. The details used in the CF-1 and CF-2 samples are the conventional details used in Iran to connect frames and infill walls.

In the CF-3 sample, the infill wall was thoroughly detached from the main frame using a secondary metallic frame. The wall's separating frame, which was built using the UPA 120 profile, was composed of two vertical elements and a horizontal element. The vertical members of the separating frame were 50 mm apart from the main frame on both sides and were completely annexed to the baseplates at the bottom. The horizontal upper member of the separating frame was 150 mm away from the beam of the main frame. The connection between the main and the secondary frames was furnished by two ADAS plates with the dimensions $150 \times 120 \times 10$. One end of the plates was attached to the beam of the main frame and the other was connected to the top of the horizontal member of the secondary frame. The pure width of the ADAS connecting plate in its midsection was chosen to be 50 mm (Fig. 1).

To build the infill walls, an experienced mason was put to work and all the bricks were fully soaked in water. All of the vertical and horizontal joints between the bricks were completely filled with mortar and watering and curing of all the samples were continued in suitable conditions until the required strength for the test was achieved. All the samples with infills were tested seven days after the masonry walls were constructed.

2.2 Experiment Setup

The details of how the experiment was conducted including loading, lateral bracing, and the measuring systems are depicted in Fig. 2. The tests were carried out in the structural lab of the Islamic Azad University

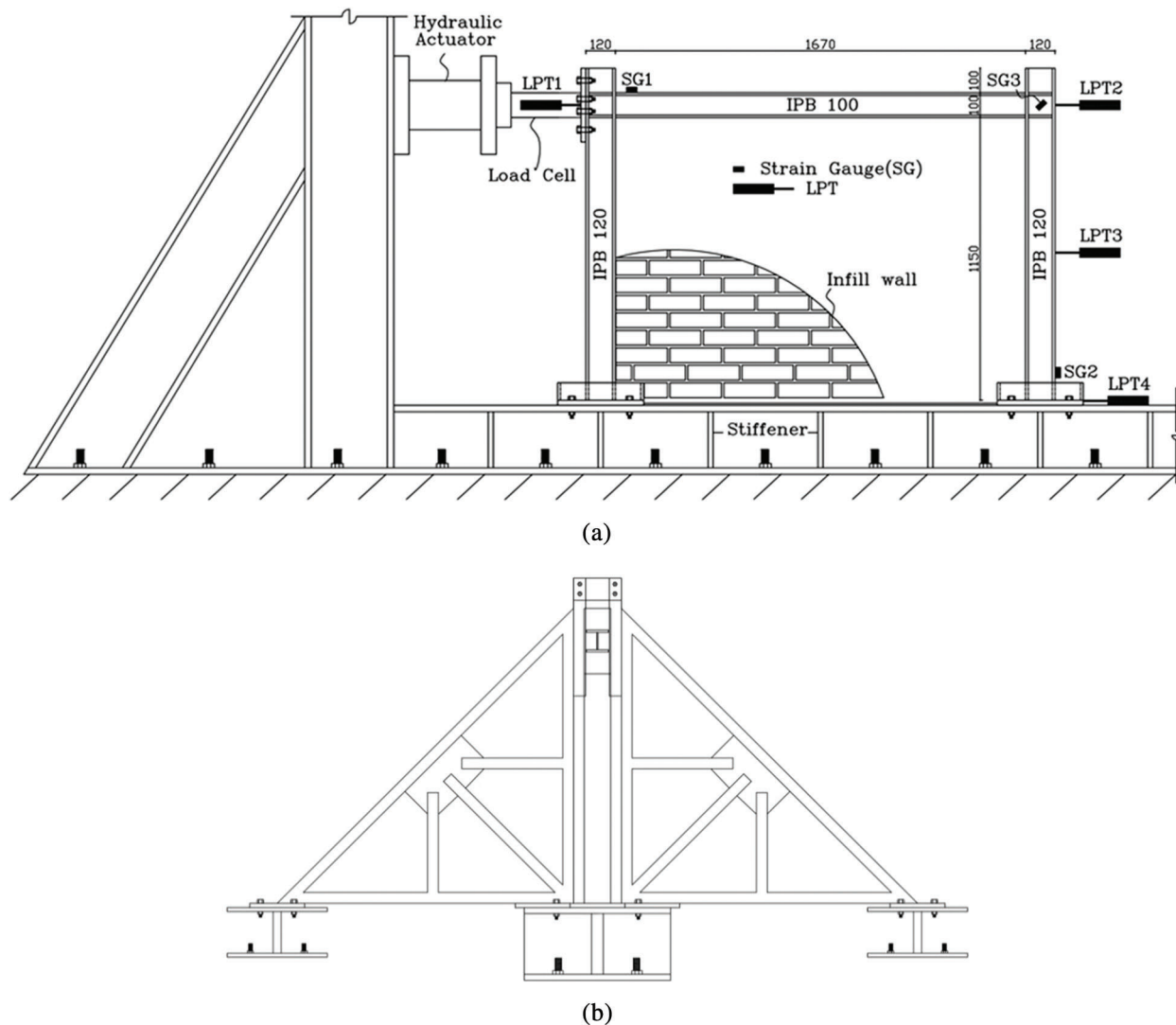


Figure 2: Test setup. (a) Schematic view. (b) Out-of-plane brace

of Kermanshah. The lateral load was applied to the beam on one side of the frame using an actuator with the capacity of 1500 kN. The static load was applied uniformly using the displacement-control method. The lateral displacements of the samples were gauged with four Linear Potentiometer Transducer (LPT) sensors which were placed on the upper corner of the frame, the mid-height of the column, and the base of the column (to restrain the possible slippage of the frame). Three strain gauges were also lodged on the upper web of the beam at the location where the beam meets the column, on the web of the column at the location where the column connects to the baseplate, and finally in the panel zone.

The frames were placed on a very strong chassis which was completely fixed to the footing beneath it using multiple bolts. All of the samples were barred from out-of-plane movements using four trusses on both sides of the beam. A 32-channel data logger was used to record the data and the values for force, displacement, and strain on different points of the frame were recorded. In this study, loading was continued until a high drift so that the behaviors of the frame, the wall, and the connection between them could be studied at the moment of collapse. Loading continued until the drift of 20% and, after obtaining the load displacement diagram of each frame, the equivalent bilinear diagram was drawn in

accordance with the FEMA 356 [2] guideline. The values for effective stiffness, strength, and ductility were also calculated.

2.3 Material Properties

The bricks used in the experiments are imperforated clay bricks widely used in Iran which were tested based on the ASTM C-67 [25] standard and the average compressive strength of five brick samples was determined to be 24.7 MPa. The volume ratio of the mortar used in the construction of the infill walls was 1:4 (one unit of cement and four units of sand), with the cement type being Portland type 2. The average compressive strength of six cubic samples of mortar with the dimensions was obtained equal to 11.0 MPa based on the ASTM C-109 [26] standard. The compressive strength of the masonry prism was measured based on the ASTM C-1314 [27] standard and the average of the compressive strength of the prismatic samples (three rows of brick and two layers of mortar) was calculated to be 11.6 MPa.

The modulus of elasticity of masonry walls is usually calculated by measuring the strain and the stress of the masonry sample and various methods on how to carry out the test and how to measure the mentioned parameters have been proposed. In accordance with the FEMA 306 [1] standard, in case experiment is not carried out, the modulus of elasticity of the masonry wall under compression can be assumed 550 times greater than the compressive strength of the material. Also, in the absence of experimental data, the tensile strength of masonry is usually presumed 10 times greater than its compressive strength Combescure et al. [28].

Despite the fact ASTM has not proposed a method to calculate the shear strength terms of the masonry wall, numerous approaches have been developed by researchers to approximate these terms. In this study, to calculate the cohesion and the friction coefficient, the equations introduced by Jukes et al. [29,30] were employed and so, the shear strength between the brick and the mortar and the friction coefficient of the contact surface were obtained to be 0.44 MPa and 0.71 MPa, respectively. The material specifications of the infill wall are presented in Tab. 2.

Table 2: Material properties of the infill wall

	Compressive strength (Mpa)	Tensile strength (Mpa)	Modulus of elasticity (Mpa)	Shear strength (Mpa)	Friction coefficient
Brick	24.7	2.47	13585	–	–
Mortar	11	1.1	6050	–	–
Wall	11.6	1.16	6380	0.44	0.71

Based on the ASTM A370 [31] standard, the tensile test was performed on the webs and flanges of the IPB 120, IPB 100, and UPA 120 profiles and the values for the modulus of elasticity, yield stress, ultimate stress, and ultimate strain were obtained. The results are given in Tab. 3.

3 Results of Experiment

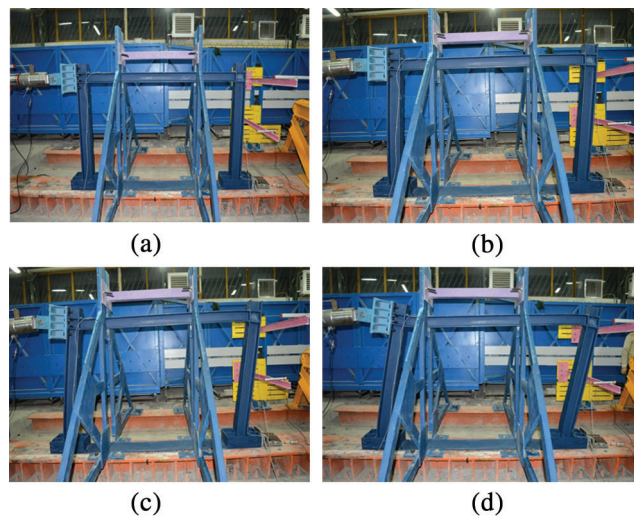
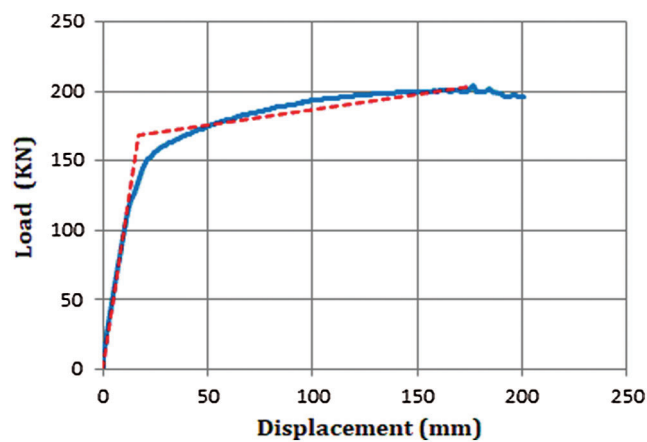
3.1 The BF Sample

The first tested sample was a steel frame without an infill wall. Fig. 3 depicts the BF sample before loading and also at the drifts 5%, 10%, 15%. The load-displacement diagram of the BF frame and also the equivalent bilinear diagram are shown in Fig. 4.

The frame had an initial stiffness of 9.69 kN/mm and as displacement in the frame increased, the stiffness drastically declined and at the yield point, reached 0.155 kN/mm. According to the load-displacement diagram, the sample begins to yield at 18.5 mm of displacement (equal to 1.54% of drift). At the moment of yielding, the strain in strain gauges 1, 2, and 3 and the strength of the frame were

Table 3: Material properties of the steel frame

Section	Coupon location	Module of Elasticity (GPa)	Yield strength, F_y (Mpa)	Tensile strength, F_u (Mpa)	Elongation (%)
IPB120	Flange	202	398.2	588.5	20.18
	Web	196	387.7	579.6	19.62
IPB100	Flange	191	401.6	624.5	25.30
	Web	193	406.1	617.9	24.14
UPA 120	Flange	198	301.2	466.8	27.12
	Web	189	291.3	440.2	27.18

**Figure 3:** The BF sample. (a) View of the frame before loading. (b) 5% of drift. (c) 10% of drift. (d) 15% of drift**Figure 4:** Load-displacement diagram of the BF frame

equal to 72E-5, 88E-5, 131E-5, and 179.25 kN, respectively. As yielding started in the sample, plastic hinges started to form in the beam, near the support and at the base of the column which was followed by the coloring of these areas falling off. The strength of the frame was equal to 203.7 kN which corresponded to 176.5 mm of displacement (equal to 14.7% of drift). The test was halted when twisting and buckling were seen in the beam and the column.

The ductility of this frame ($\Delta u/\Delta y$) was 9.54. To assess the energy absorption capability and the ductility of the frame, the Energy Dissipation of the frame up until the Top Shear value (EDTS) and the energy dissipation of the frame at the final drift (Total Energy Dissipation—TED) were calculated based on the area beneath the load displacement-diagram. In addition to the fact that the values of TED and EDTS both represent energy dissipation in the frame, the EDTS/TED ratio, similar to the $\Delta u/\Delta y$ ratio, can also be used as an index with which to evaluate the ductility of the samples. It is evident that a higher value of this index indicates higher ductility and higher energy absorption and energy dissipation by the frame, without any decline in the load-displacement diagram. The total energy absorbed by the BF sample and the energy absorbed up to the maximum amount of load are equal to 35.8 kJ and 31.2 kJ, respectively. Therefore, the EDTS/TED ratio for this frame is 0.87.

3.2 SF Sample

The next sample was a frame that incorporated an infill wall without any secondary connection between the wall and the frame. In other words, the only connection between the frame and the infill was supplied by the physical contact between the infill wall (the mortar and the bricks) and the column. Fig. 5 displays the condition of the SF sample before loading, crack expansion, and also the condition of the wall in different stages of loading.

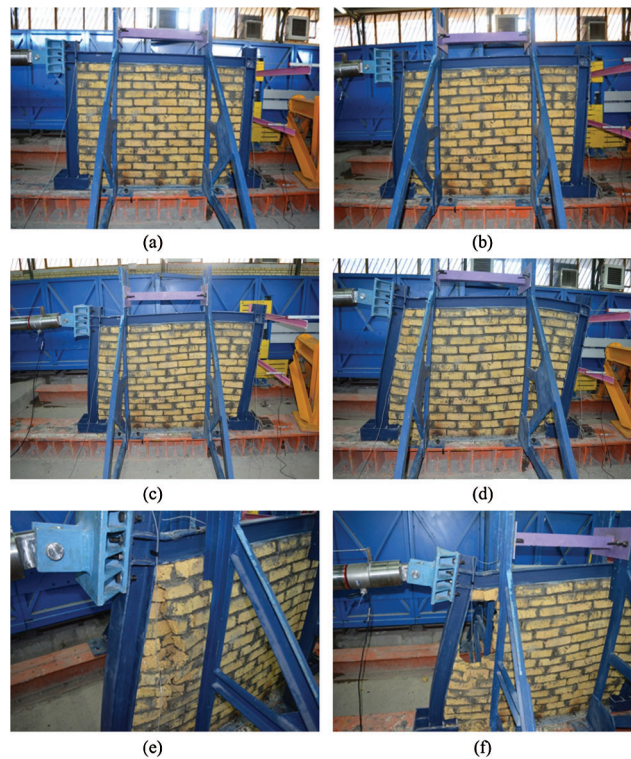


Figure 5: The SF sample. (a) View of the frame before loading. (b) 5% of drift. (c) 10% of drift. (d) 15% of drift. (e) Cracking of the compressive corner of the infill. (f) Plastic deformation of the column and the beam

As loading initiated and at a displacement of 10 mm, a thin oblique crack started to form along the compressive diagonal of the wall which developed a staircase shape in the vertical and horizontal joints. By increasing displacement, due to the interaction between the frame and the infill, the midsection and the right half of the wall started to move upward and applying pressure to the beam caused the beam to also move upward. A similar behavior was previously reported by Achyutha [32] and Riddington [33].

At 40 mm of displacement, a vertical crack started to develop in the right side, from beneath the beam to the diagonal crack in the panel. In the left half of the wall and along the compressive diagonal, the end of the bricks started to tend downward and in the right half, the end of the bricks leaned upward and this caused the vertical wave to take form in the brick rows of the wall. Because of the tendency of the infill to react with the beam, the vertical displacement of the beam was similar to the deformation of the brick rows of the wall.

Fig. 6 displays the load-displacement diagram and its corresponding equivalent bilinear diagram. The frame has an initial stiffness of 12 kN/mm. As displacement of the frame increased, the stiffness of the frame decreased and at the point at which the sample started to yield, the stiffness reached 0.614 kN/mm. According to the displacement diagram, the sample started to yield at a displacement of 18.9 mm (1.58% of drift). At the moment of yielding, strain in strain gauges 1, 2, and 3 and the strength of the frame in the yield limit was equal to, 63E-5, 31E-5, 32E-5, and 227 kN, respectively. The maximum load in this frame is 286 kN which corresponds to 114.7 mm of displacement (9.56% of drift). At this displacement, the crushing of the upper left corner of the panel of the infill and also the expansion of vertical and diagonal cracks was observed resulted in a drastic strength reduction and the load-displacement diagram. Also, after this stage, due to the absence of any anchor between the infill wall and the frame, out-of-plane deviation of the frame's panel was observed. In addition, the bricks of the upper left corner were crushed and smashed. At the displacement of 200 mm (16.6% of drift) the corner of the infill, due to severe crushing, fell down and the test was stopped.

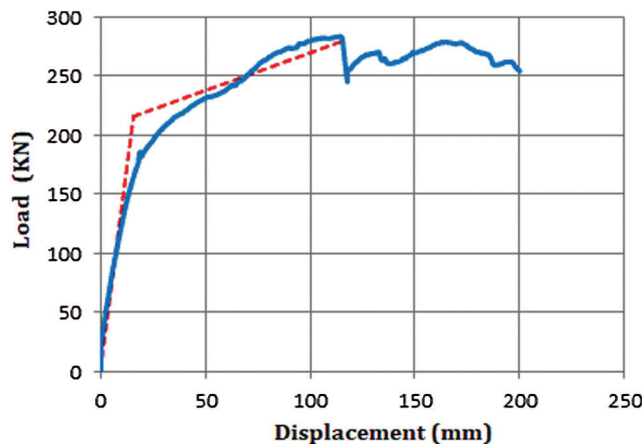


Figure 6: Load-displacement diagram of the SF frame

The ductility of this frame is 6.07 and the values of TED and EDTS are equal to 48.5 kJ and 25.7 kJ, respectively. Although the total energy dissipation in the SF model is larger than that of the BF model, the EDTS/TED index for this frame is equal to 0.53 which denotes a more rapid decline in the envelope diagram and a lower ductility.

3.3 CF-1 Sample

A very simple and practical idea to separate the infill panel from the frame and also to brace the infill wall and prevented from deviation and out-of-plane downfall is to use vertical angles on both sides of the infill panel and this was tested in the third sample. In each of the angles, one side acted as a brace to prohibit

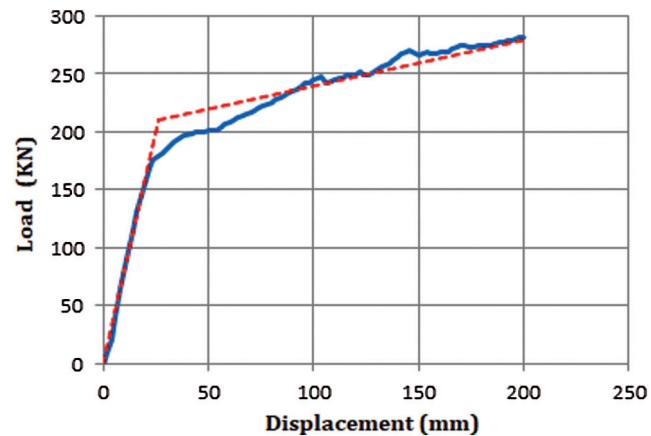


Figure 7: Load-displacement diagram of the CF-1 frame

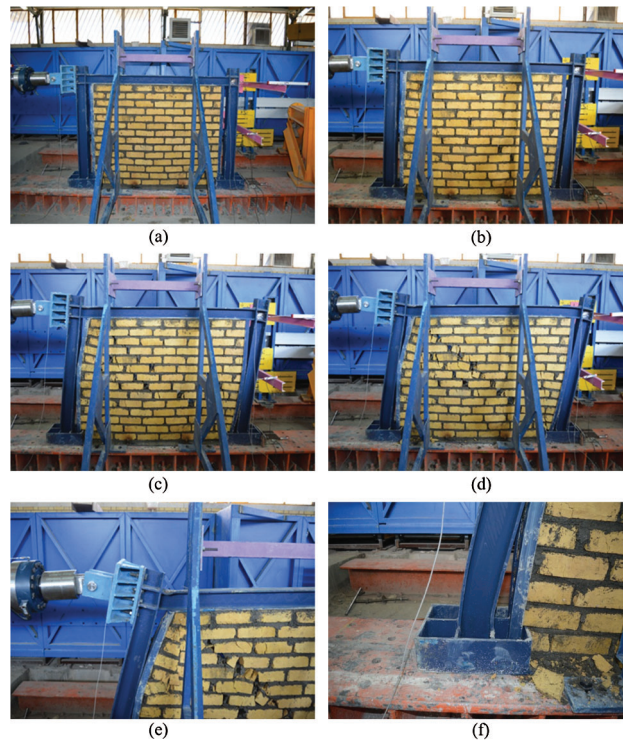


Figure 8: The CF-1 frame. (a) View frame before loading. (b) 5% of drift. (c) 10% of drift. (d) 15% of drift. (e) Crushing of the compressive corner of the infill and the plastic deformation of the beam. (f) Plastic deformation of the column

in-plane movement and the other side prevented the wall from its out-of-plane displacement. The load displacement diagram of the frame and its corresponding equivalent bilinear diagram are presented in Fig. 7 and the crack expansion pattern and the failure modes of the frame are illustrated in Fig. 8.

At the displacement of 15 mm (1.25% of drift) the first crack was created in the panel of the infill. The crack, in the vertical and horizontal joints of the masonry infill, continued to expand from the top left corner of the panel, in an angle close to 45° , towards the lower right corner following an oblique and staircase

pattern. As the displacement of the frame increased, the width of the crack enlarged at any moment. At the displacement of 30 mm (2.5% of drift), another crack, parallel to the first one, was developed. Contrary to the first crack which developed in the vertical and horizontal mortar joints of the wall, the second crack primarily went through the bricks and the vertical mortar joints. As the displacement continued and the width of the crack widened, the angles on both sides in-planely displaced in a crescent-shape way and from their midpoints, drew closer to the columns. At the displacement of 58 mm (4.83% of drift), as the in-plane arc of the angles on both sides increased, a third crack initiated from the upper end of the second crack and vertically continued downward to the middle of the height of the wall.

In this sample, as well, an upward movement was observed in the right half of the wall, but it was smaller than the one seen in the previous sample which indicates that the wall is less inclined to push against the beam. Therefore, the vertical displacement of the beam in this sample is smaller. Furthermore, in this sample, the out-of-plane displacement of the wall has been sufficiently restricted by the angles.

Applying displacement to the sample continued until 200 mm (16.6% of drift) and the frame still displayed increasing strength. A maximum load of 285 kN was reached at the displacement of 200 mm and the yield limit was recorded equal to 218.2 kN. The width of the crack continued to grow until the end of loading but no crushing was seen in the corners of the panel of the infill. The initial stiffness of the frame was 8.19 kN/mm and in the point at which yielding initiated (26.65 mm of displacement equal to 2.22% of drift), it lessened by 0.385 kN/mm. at the moment of yielding, the amount of a strain in strain gauges 1, 2, and 3 was recorded equal to 139E-5, 205E-5, and 142E-5, respectively.

The ductility of the sample and the total absorbed energy was obtained equal to 7.5 kJ and 44.7 kJ, respectively. Considering that no decline was seen in the envelope diagram, the EDTS/TED ratio for this frame is 1. The test was stopped when the welding of the angles failed.

3.4 CF-2 Sample

Another simple and practical solution for bracing and connecting the wall to the infill is using steel rebars with a 90° bend on both ends. These rebars can be effective in bracing the wall from in-plane and out-of-plane displacements. This idea was tested in the fourth experiment and different stages of loading are given in Fig. 9.

The first thin crack was created in the panel of the infill at 36 mm of displacement (3% of drift). The delayed crack formation compared to the other samples was due to the existence of the rebars that connected the frame to the infill which also caused the change in the crack expansion pattern and the failure mode of the wall. The direction along which this crack was formed and expanded was from the middle of the wall in the lower section to the upper left corner of the wall, through the bricks and the vertical mortar joints.

Also, upward movement of the right section of the wall was observed which caused vertical displacement in the beam. However, the upward movement of the wall was smaller compared to the other samples. As the loading continued and at a displacement of 86 mm (7.17% of drift), bricks started to peel off in the midsection of the path of the crack and at a displacement of 112 mm (9.33% of drift), a portion of the peel off section fell off. After this stage, some scattered vertical cracks were observed in the bricks of the right side, however, the collapse concentration in the wall was in the part with the peel off bricks which finally resulted in local failure and the creation of a hole in the wall. In this sample no crushing of the corners was observed. At the end of the test, the out-of-plane displacement of the wall in its midsection was measured equal to 60 mm. The test was halted when the wall went through local failure and the wall and the frame experienced excessive deformations. The maximum load in the frame was 288.7 kN which was reached at a displacement of 80 mm (6.67% of drift).



Figure 9: The CF-2 frame. (a) How the bracing rebars are added. (b) View of the frame before loading. (c) 5% of drift. (d) 10% of drift. (e) 15% of drift. (f) Final deformation of the frame

According to the load-displacement diagram shown in Fig. 10, the initial stiffness of the frame and the decreased stiffness at the moment when yielding began are equal to 8.78 kN/mm and 1.02 kN/mm, respectively. Yielding of the sample initiated at a displacement of 26.7 mm (2.22% of drift) and the yield strength of the sample was equal to 234.4 kN. At the moment of yielding, strain in strain gauges 1, 2, and 3 was equal to 233E-5, 60E-5, and 148E-5, respectively.

The ductility of the frame is 2.99 which, compared to the other frames, is lower. The total energy absorbed by the frame, the dissipated energy until the moment of maximum load, and the EDTS/TED ratio are 48.6 kJ, 16.8 kJ, and 0.35 kJ, respectively.

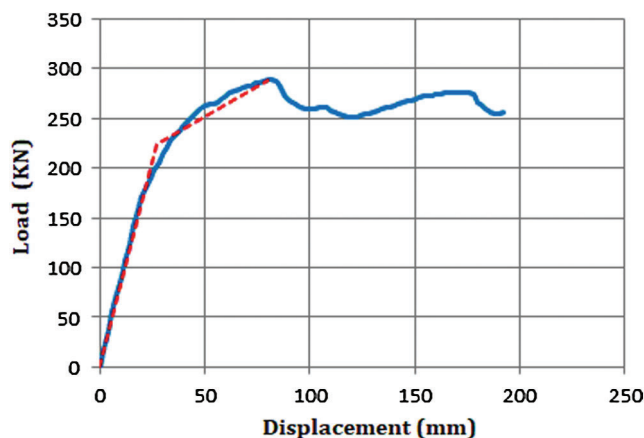


Figure 10: Load-displacement diagram of the CF-2 frame

3.5 CF-3 Sample

In the last sample, the infill wall was braced using a secondary frame and was completely enclosed on three sides in the connection between the frames was supplied by ADAS plates with low thickness. In addition to bracing the infill wall against in-plane and out-of-plane deformations, the secondary frame also delays the wall from being damaged (Fig. 11). So, the lateral stiffness of the wall can be taken advantage of but energy dissipation can be concentrated in a replaceable component like the ADAS dampers.

The dimensions and the thickness of the ADAS plates were selected in such a way so that they yield under the effect of lateral force and enter the plastic phase. A strain gauge was also placed on the narrowest section of the ADAS element. At the beginning of loading, due to the lack of direct connection between the main and the secondary frames, most of deformation and energy dissipation were concentrated in the connecting plates and a significant displacement was not laid upon the wall. At 50 mm of displacement (4.17% of drift), the first connection was established between the main frame and the secondary frame and immediately thereafter, the first crack formed in the wall. The direction of this oblique crack was at approximately 1/4 of the height of the column on the lower right corner to a point roughly 1/4 of the span of the wall from the upper left corner of the wall.

As loading continued, the width of the crack grew proportional to the displacement being applied. Deformation in the columns of the secondary frame was of a crescent-like shape, accompanied by mid-height protrusion of the columns. In this condition, by the upward displacement of the wall, the beam of the secondary frame also experienced vertical displacement. At 98 mm of displacement (8.17% of drift), a second crack was created in the mid-span of the wall at the bottom and, almost parallel to the first crack, continued to grow toward the upper left corner of the wall.



Figure 11: The CF-3 frame. (a) View of the frame before loading. (b) Connecting plates. (c) 5% of drift. (d) 10% of drift. (e) 15% of drift. (f) Final deformation of the frame

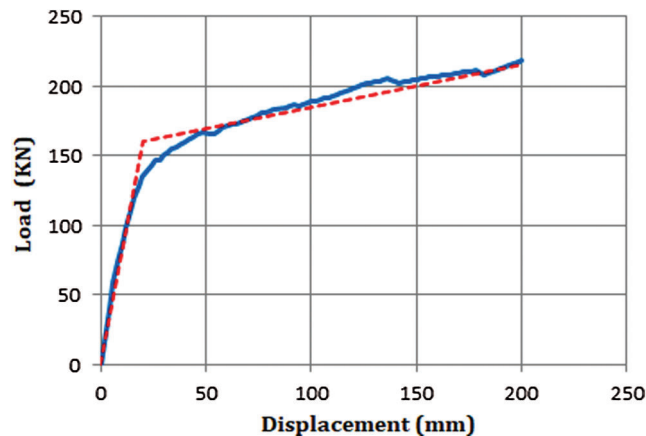


Figure 12: Load displacement diagram of the CF-3 frame

Loading was continued until 16.6% of drift. The load displacement diagram and the bilinear equivalent diagram of the frame are shown in Fig. 12. The maximum load of the frame was 218.1 kN which corresponded to 200 mm of displacement (16.6% of drift). At 16.6% of drift, tearing in the beam of the secondary frame and large displacements in the beam and the column of the main frame were observed, whereupon the test was stopped.

The initial stiffness of the sample, stiffness at the moment yielding began, strength, and drift at the moment of yielding were recorded equal to 8.23 kN/mm, 0.3 kN/mm, 164 kN, and 19.93 (16.6% of drift), respectively. At the moment of yielding, strain in strain gauges 1, 2, and 3 were equal to 68E-5, 46E-5, and 99E-5.

The energy absorbed until the moment of maximum load was 35.6 kJ which equals the total energy absorbed by the frame. The EDTS/TED ratio for this frame is equal to 1 and the ductility factor is equal to 10.03 which is higher than the other samples.

4 Results and Discussion

The load displacement diagrams of all the samples are illustrated in Fig. 13. Based on the envelope diagram, the equivalent bilinear diagram, and experimental observations, the seismic specifications of all the five samples are given in Tab. 4.

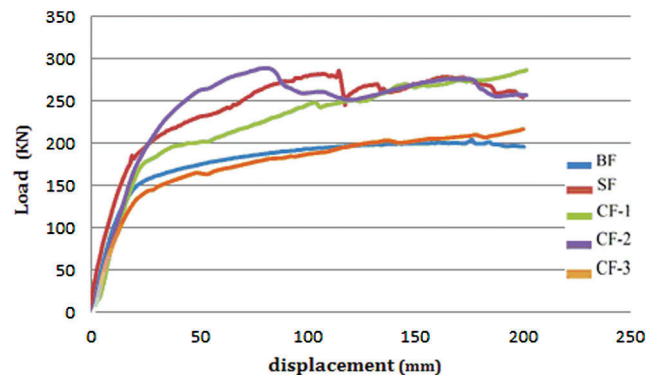


Figure 13: Load-displacement diagrams of all the samples

Table 4: The response of the experimental samples

Sample	Initial stiffness (kN/mm)	Displacement corresponding to the creation of the first crack (mm)	Yield Strength (kN)	Ultimate Load (kN)	Drift Corresponding to the ultimate load (%)	Ductility TED (kJ)	EDTS/TED
BF	9.69	–	179.25	203.7	14.7	9.54	0.87
SF	12	10	227	286	9.56	6.07	0.53
CF-1	8.19	15	218.2	285	16.67	7.5	1
CF-2	8.78	36	234.4	288.7	6.67	2.99	0.35
CF-3	8.23	50	164	218.1	16.67	10.03	1

Compared to the BF sample, the SF sample has 23.8% higher initial stiffness, 26.6% higher yield strength, and 40.4% higher ultimate load. Also, the energy dissipation of the SF sample is about 35% higher than that of the BF sample. Compared to the BF sample, the ductility and the EDTS/TED ratio of the SF sample have decreased by 36.4% and 39.1%, respectively. It is obvious that the existence of the infill wall causes the stiffness and the strength of the frame to increase, however, it decreases its ductility. Therefore, the direct interaction between the frame and the infill wall can improve the performance of the structure during weak or average earthquakes.

It has to be said, however, that during strong earthquakes, due to the decreased ductility of the structure and a sudden decline in the load displacement diagram, a brace-less direct connection between the infill wall and the frame can have undesirable effects on the behavior of the structure. In two of the samples, the CF-1 and especially the CF-2, this deficiency has been significantly surmounted.

Compared to the other samples, the SF sample has the highest initial stiffness. In the three samples CF-1, CF-2, and CF-3, a decrease in the initial stiffness is observed. Despite the effective stiffness decreasing, no decrease has been seen in energy dissipation and it has significantly increased in the CF-1 and CF-2 samples. The EDTS/TED ratio in the CF-1 and CF-3 samples is equal to 1 which is indicative of no decline happening in the envelope diagram and the good performance of these two samples.

Comparing the ductility of the frames shows that the CF-1 and CF-3 frames, due to the complete separation of the panel of the infill from the wall and the complete anchoring of the wall, have a higher ductility compared to the other samples. The CF-2 sample, despite having the highest strength, displayed the lowest ductility due to the reinforcement of the wall and restricting its displacement by connecting it to the frame.

Crack formation of the infill wall in the CF-1, CF-2, and CF-3 samples happened later compared to the SF sample. By evaluating the displacements that resulted in crack formation and damage to the wall, it was revealed that the CF-3 sample has the highest displacement capacity without considerable damage being inflicted on the wall. Even after the columns hitting the wall, the secondary frame, with its good performance, braced the wall and prevented damages that could result in the collapse of the wall. In Fig. 14, crack formation patterns and the failure modes of the wall in each of the samples are shown. Comparing the failure modes of the samples reveals that the existence and nonexistence of connection between the frame and the infill and also the type of the connection, influences the way in which the wall fails. In the SF and CF-2 samples, which have a higher stiffness and a lower ductility compared to the other samples with infills, the damage in the wall is higher and even at the final displacement, local

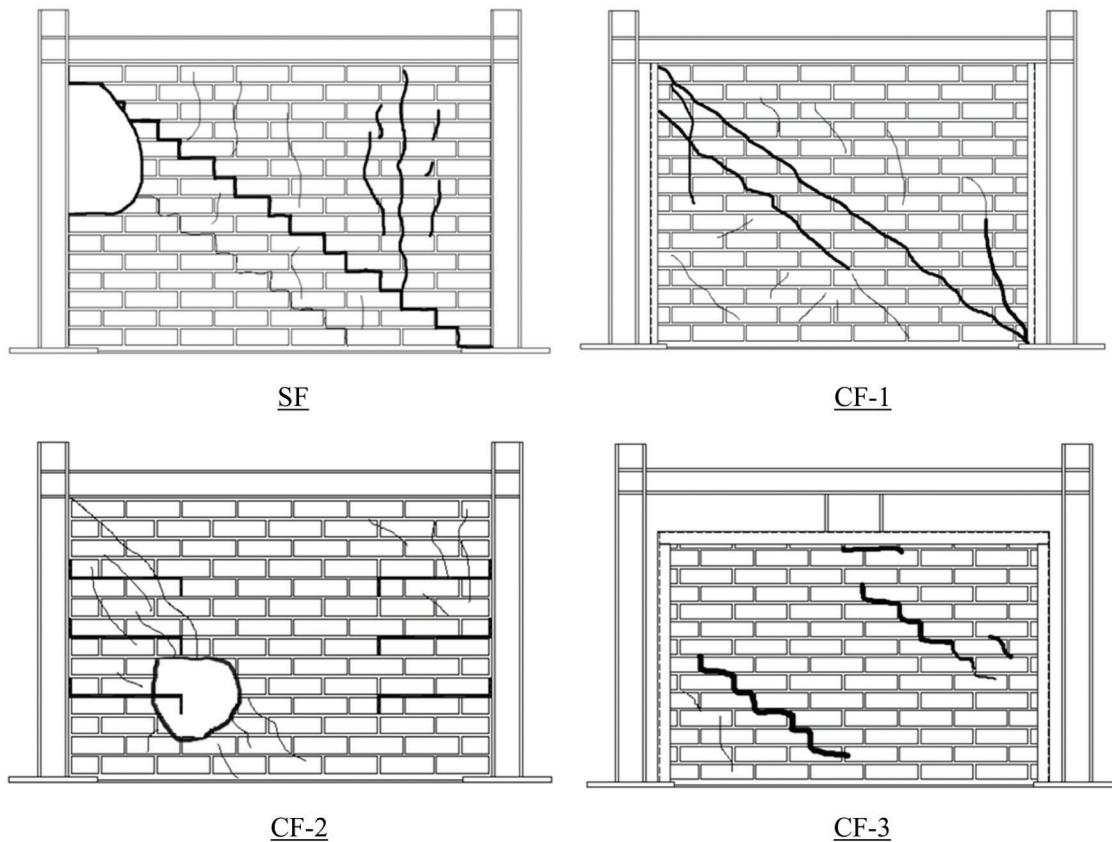


Figure 14: Comparison between crack formation patterns and the failure modes of the infill

failure occurred. But, in the two samples CF-1 and CF-3, which have higher ductility, the level of damage inflicted on the wall is small.

In the SF sample, which does not incorporate any kind of connection between the frame and the infill, crushing of the corners and the vertical cracks formed by the upward movement of the wall occurred. In the CF-1 sample, in which the infill wall was braced to the frame using vertical angles, due to the resemblance of the behavior of the angles to that of the column, the pattern in which cracks started to form was diagonal at the initial stages of loading. But, due to the flexibility and deformation of the angle, damage was not inflicted on the corners and local collapse did not take place as displacement increased in the frame. In addition, the angles completely braced the wall from out of plane displacement. The steel rebars used to embrace the wall to the frame in the CF-2 sample caused the crack formation pattern to change from a diagonal shape and move further downward. In this sample, the out of plane displacement was significant but until the end of loading, the rebars properly prevented the collapse of the wall. In the CF-3 sample, crack formation pattern was thoroughly different and short oblique cracks took form in the vicinity of the corners. Furthermore, despite the large displacement of the frame, the stability of the wall was fully preserved and no kind of local or universal collapse of the wall was observed. Also, the out of plane displacement of the wall in this sample was quite negligible.

Fig. 15 presents the strain in the compressive flange of the beam, the compressive flange of the column, and the panel zone. Fig. 15a illustrates that in the frame without an infill, the maximum strain in the compressive flange of the beam is smaller compared to the other samples. The highest strain in the compressive flange of the beam belonged to the CF-1 sample which is probably due to the vertical angles

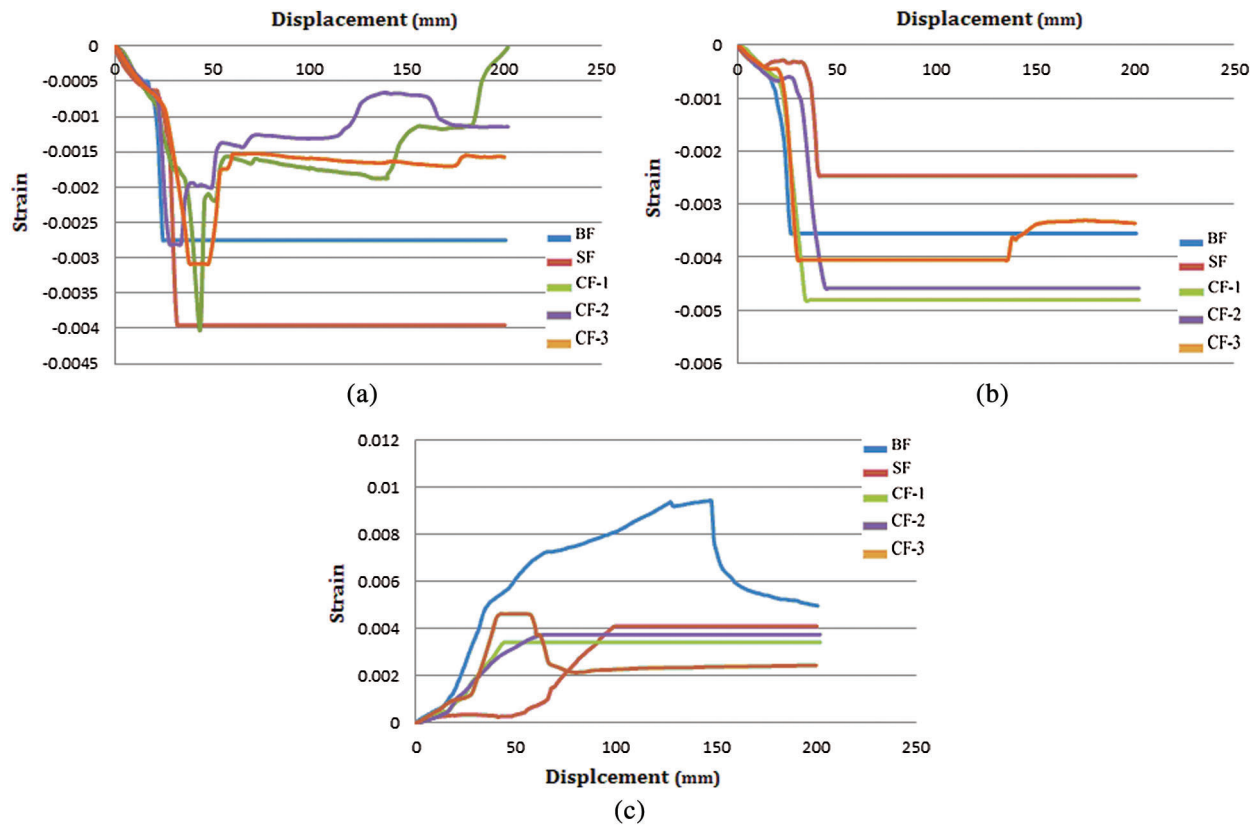


Figure 15: Strain diagrams. (a) Compressive flange of the beam. (b) Compressive flange of the column. (c) Panel zone

and the beam being connected and the transference of the forces from the brace of the wall to the beam. From the shape standpoint, the changes of strain in the compressive flange of the beam in the BF and SF samples are similar to one another but the amount of strain in the SF sample is larger than the BF sample. The strain in the compressive flange of the beam in all samples exceeded the yield limit and the strain in the samples SF and CF-1 was larger compared to the rest of the samples.

The changes of strain in the compressive flange of the column is shown in Fig. 15b. The lowest amount of strain in the compressive flange of the column belongs to the SF sample. In this sample, because of the diagonal distribution of compressive force in the panel of the infill, strain at the base of the column is lower. Amongst the samples CF-1, CF-2, and CF-3, the lowest strain in the flange of the column belongs to the CF-3 sample.

The panel zone of the beam-to-column connection is inside the column. This region is very influential in the behavior of the steel moment resisting frame against earthquake. Fig. 2 shows the exact installation location of the strain gauge in the panel zone. The presence of the infill drastically decreases the strain of the panel zone. This can be clearly seen in the diagram shown in Fig. 15c. The panel zone of the BF sample has the highest strain and the CF-1 frame has the lowest strain. The highest panel zone strain occurred in the SF sample which took place at 96 mm (8% of drift) of displacement. Prior to significant damage being inflicted upon the infill wall, the amount of strain is very small but with the cracking of the wall increasing and it's the stiffness significantly decreasing, the strain of the panel zone increases as well. In the CF-3 sample, the strain of the panel zone is initially higher than those of the CF-1 and CF-2

samples. However, with displacement increasing and the main and the secondary frames crashing into each other, the strain in this section follows a declining and reduces.

The conventional details for connecting the infill wall to the frame in Iran are the CF-1 and CF-2 samples and it can be said that the behavior of the CF-1 sample is better and at a satisfactory level. The behavior of the CF-3 sample is better than that of the other samples and choosing the appropriate thickness for the ADAS plates can have a direct effect on the stiffness and the strength of the frame. The thickness has to be chosen in such a manner so that the ADAS plate yields before damage is inflicted on the wall. At the same time, the highest possible thickness has to be selected to increase the stiffness and the strength of the frame. The superiority of this type of connection can be summarized in the followings:

- Increasing the ductility of the frame.
- No decline in the envelope diagram.
- Effective utilization of the stiffness and the strength of the wall without any damage occurring during weak and average earthquakes.
- Damage concentration in the ADAS plates in weak and average earthquake and the ability of these components to be replaced.

5 Conclusions

In this paper, an experimental study to evaluate the behavior of masonry infill walls connected, with different details, to steel frames of the scale 1:3 is presented. The experimental samples included a sample with a direct connection between the infill wall and the frame, a sample in which the infill wall was connected to the frame using vertical separating angles, a sample with embedded steel rebars in the wall, and a sample in which a secondary frame and ADAS plates were used. All five samples were subjected to monotonic and quasi-static in-plane lateral load. Some of the most important results interpreted from this experiment are:

1. The presence of the masonry infill with a direct connection to the frame cause due stiffness, the ultimate strength and the energy dissipation of the frame increased by 23.8%, 40.8%, and 35%, respectively. Also, the presence of the infill caused ductility to decrease by 36.4% and also brought about a decline in the envelope diagram.
2. Compared to the SF sample, the effective stiffness of the CF-1, CF-2, and CF-3 samples is between 25% and 30% lower. The strengths of the CF-1 and CF-2 samples are similar to the strength of the SF sample.
3. The type of the connection between the frame and the infill is extremely influential in the overall ductility of the frame. The ductilities of the CF-1 and CF-3 samples are respectively 23.6% and 65.2% higher compared to the SF sample and no decline was observed in the envelope diagram.
4. Analyzing the models shows that changing the details of the connection between the infill and the frame changes the crack formation pattern and the failure modes of the wall.
5. The recommended details for the connection between the infill and the frame bring about a considerable decrease in the strain of the compressive flange of column and the panel zone and an increase in the strain of the compressive flange of the beam. Therefore, in the design of frames and their connections, it seems necessary to take into account these local effects.
6. The behavior of the CF-3 sample was better compared to the other samples and choosing the appropriate thickness for the ADAS plates can directly affect the stiffness and the strength of the frame. This thickness has to be chosen in such a way so that the ADAS plates yield before the wall is damaged and at the same time the highest possible thickness has to be chosen in order to increase the stiffness and the strength of the frame. The superiority of this type of connection lies in the following factors: increasing the ductility of the frame, no decline taking placed in the envelope diagram, effective utilization of the stiffness and the

strength of the wall, damage concentration in the ADAS plates in weak and average earthquakes, and the replace-ability of these components. Thus, it is recommended to use these details in bracing the panel of the infill in special moments resisting frames in regions with high seismic risk.

Acknowledgement: The authors would like to gratefully thank the structural research lab of the Islamic Azad University of Kermanshah and the Omran-Sazeh Company.

Funding Statement: The author(s) received no specific funding for this study.

Conflicts of Interest: The authors declare that they have no conflicts of interest to report regarding the present study.

References

1. Federal Emergency Management Agency. (1998). *Evaluation of earthquake damaged concrete and masonry wall buildings*. Report no. FEMA 306. Washington, DC: FEMA.
2. Federal Emergency Management Agency. (2000). *Prestandard and commentary for the seismic rehabilitation of buildings*. Report no. FEMA 356. Washington, DC: FEMA.
3. Smith, B. S. (1962). Lateral stiffness of infilled frames. *Journal of the Structural Division*, 88(6), 183–226.
4. Smith, B. S. (1966). Behavior of square infilled frames. *Journal of the Structural Division*, 92(1), 381–404.
5. Moghaddam, H. A., Dowling, P. J. (1987). *The state of the art in infilled frames*. London: Imperial College of Science and Technology, Civil Engineering Department.
6. Abrams, D. P. (1994). *Proceedings from the NCEER workshop on seismic response of masonry infills*. London: NCEER.
7. Calvi, G. M., Santini, S. (1996). Experimental and numerical investigations on the seismic response of RC infilled frames and recommendations for code provisions. In ECOEST-PREC8, Report n.6. <http://hdl.handle.net/11590/169323>.
8. Crisafulli, F. J., Carr, A. J., Park, R. (2000). Analytical modelling of infilled frame structures—a general review. *Bulletin-New Zealand Society for Earthquake Engineering*, 33(1), 30–47. DOI 10.5459/bnzsee.33.1.30-47.
9. Moghadam, H. A., Mohammadi, M. G., Ghaemian, M. (2006). Experimental and analytical investigation into crack strength determination of infilled steel frames. *Journal of Constructional Steel Research*, 62(12), 1341–1352. DOI 10.1016/j.jcsr.2006.01.002.
10. Puglisi, M., Uzcategui, M., Flórez-López, J. (2009). Modeling of masonry of infilled frames, part I: the plastic concentrator. *Engineering Structures*, 31(1), 113–118. DOI 10.1016/j.engstruct.2008.07.012.
11. Puglisi, M., Uzcategui, M., Flórez-López, J. (2009). Modeling of masonry of infilled frames, part II: cracking and damage. *Engineering Structures*, 31(1), 119–124. DOI 10.1016/j.engstruct.2008.07.013.
12. Mohammadi, M., Akrami, V. (2010). An engineered infilled frame: behavior and calibration. *Journal of Constructional Steel Research*, 66(6), 842–849. DOI 10.1016/j.jcsr.2010.01.008.
13. Bayat, M., Abdollahzade, G. R. (2011). Analysis of the steel braced frames equipped with ADAS devices under the far field records. *Latin American Journal of Solids and Structures*, 8(2), 163–181. DOI 10.1590/S1679-78252011000200004.
14. Bayat, M., Abdollahzadeh, G. (2011). On the effect of the near field records on the steel braced frames equipped with energy dissipating devices. *Latin American Journal of Solids and Structures*, 8(4), 429–443. DOI 10.1590/S1679-78252011000400004.
15. Liu, Y., Manesh, P. (2013). Concrete masonry infilled steel frames subjected to combined in-plane lateral and axial loading—an experimental study. *Engineering Structures*, 52, 331–339. DOI 10.1016/j.engstruct.2013.02.038.
16. Jazany, R. A., Hajirasouliha, I., Farshchi, H. (2013). Influence of masonry infill on the seismic performance of concentrically braced frames. *Journal of Constructional Steel Research*, 88, 150–163. DOI 10.1016/j.jcsr.2013.05.009.

17. Bayat, M., Bayat, M. (2014). Seismic behavior of special moment-resisting frames with energy dissipating devices under near source ground motions. *Steel and Composite Structures*, 16(5), 533–557. DOI 10.12989/scs.2014.16.5.533.
18. Okail, H., Abdelrahman, A., Abdelkhalik, A., Metwaly, M. (2014). Experimental and analytical investigation of the lateral load response of confined masonry walls. *HBRC Journal*, 12(1), 33–46. DOI 10.1016/j.hbrj.2014.09.004.
19. Tawfik Essa, A. S. A., Badr, M. R. K., El-Zanaty, A. H. (2014). Effect of infill wall on the ductility and behavior of high strength reinforced concrete frames. *HBRC Journal*, 10(3), 258–264. DOI 10.1016/j.hbrj.2013.12.005.
20. Yuen, Y. P., Kuang, J. S. (2015). Nonlinear seismic responses and lateral force transfer mechanisms of RC frames with different infill configurations. *Engineering Structures*, 91, 125–140. DOI 10.1016/j.engstruct.2015.02.031.
21. Jiang, H., Liu, X., Mao, J. (2015). Full-scale experimental study on masonry infilled RC moment-resisting frames under cyclic loads. *Engineering Structures*, 91, 70–84. DOI 10.1016/j.engstruct.2015.02.008.
22. Furtado, A., Rodrigues, H., Arêde, A., Varum, H. (2016). Experimental evaluation of out-of-plane capacity of masonry infill walls. *Engineering Structures*, 111, 48–63. DOI 10.1016/j.engstruct.2015.12.013.
23. Basha, S. H., Kaushik, H. B. (2016). Behavior and failure mechanisms of masonry-infilled RC frames (in low-rise buildings) subject to lateral loading. *Engineering Structures*, 111, 233–245. DOI 10.1016/j.engstruct.2015.12.034.
24. Kahrizi, M., TahamouliRoudsari, M. (2019). Experimental and numerical investigation of the parameters affecting the behavior of steel frames with masonry infill walls anchored with the ADAS yielding damper. *European Journal of Environmental and Civil Engineering*, 33(1), 1–22. DOI 10.1080/19648189.2018.1543057.
25. American Society for Testing and Materials. (2002). Standard test methods for sampling and testing brick and structural clay tile. C 67–02c. *ASTM International*.
26. American Society for Testing and Materials. (2007). Standard test method for compressive strength of hydraulic cement mortars (using 2-in. or [50-mm] Cube Specimens). C 109/C 109M–07. *ASTM International*.
27. American Society for Testing and Materials. (2003). Standard test method for compressive strength of masonry prisms. C 1314–03a. *ASTM International*.
28. Combescure, D., Pegon, P. (2000). Application of the local-to-global approach to the study of infilled frame structures under seismic loading. *Nuclear Engineering and Design*, 196(1), 17–40. DOI 10.1016/S0029-5493(99)00228-9.
29. Jukes, P., Riddington, J. R. (1997). Review of masonry joint shear strength test methods. *Masonry International*, 11(2), 37–43.
30. Jukes, P., Riddington, J. R. (1998). Review of masonry tensile bond strength test methods. *Masonry International*, 12(2), 51–57.
31. American Society for Testing and Materials. (2002). *Standard test methods and definitions for mechanical testing of steel products*. Philadelphia, PA: ASTM Standard A370-02.
32. Achyutha, H. (1982). Effect of contact between infill and frame on the behaviour of infilled multistorey frames. *Proceedings of the Sixth International Brick Masonry Conference, Rome*.
33. Riddington, J. R. (1984). The influence of initial gaps on infilled frame behaviour. *Proceedings of the Institution of Civil Engineers*, 77(3), 295–310. DOI 10.1680/iicep.1984.1185.